Available online at www.sciencedirect.com
SCIENCE DIRECT®
Bioorganic Chemistry 34 (2006) 77–89
BIOORGANIC CHEMISTRY
www.elsevier.com/locate/bioorg

A semiempirical study of acetylcholine hydrolysis catalyzed by *Drosophila melanogaster* acetylcholinesterase

Carlos Mauricio R. Sant'Anna *, Andrea dos Santos Viana, Nailton Monteiro do Nascimento Junior

Departamento de Química, ICE, Universidade Federal Rural do Rio de Janeiro, RJ 23851-970, Seropédica, Brazil

Received 13 September 2005

Abstract

The enzymatic mechanism of acetylcholine hydrolysis was evaluated by semiempirical molecular orbital calculations with a model constructed with the coordinates of sixteen amino acids and four water molecules from the crystallographic structure of *Drosophila melanogaster* acetylcholinesterase (AChE, entry 1QO9 in the Protein Data Bank). Nine proposed reaction points for the hydrolysis mechanism were obtained, including four for the acylation step and five for the deacylation step. Our results indicate that in the Michaelis complex of the acylation step, a looser interaction between the substrate and the oxyanion hole may result from an amino acid change in the acyl pocket observed in insect as compared to the vertebrate enzyme. Detailed descriptions of the reaction profile for the formation of both acylation and deacylation tetrahedral intermediates were obtained. The results indicate the occurrence of partially concerted mechanisms, with deprotonation of the nucleophiles (Ser238 in the acylation step and a water molecule in the deacylation step) by His480 facilitating the nucleophilic additions. Both processes were completed by enthalpically favorable steps, formation of choline in the acylation step and of acetic acid in the deacylation step.

Keywords: AChE; *Drosophila melanogaster*; ACh hydrolysis; Mechanism; Semiempirical method

* Corresponding author. Fax: +55 21 26821872.
E-mail address: santanna@ufrrj.br (C. M. R. Sant'Anna).

0045-2068/$ - see front matter © 2006 Elsevier Inc. All rights reserved.
doi:10.1016/j.bioorg.2006.01.002

1. Introduction

The control of insect pest species plays a major role in crop production and public health. Crop losses worldwide due to insects have been estimated to amount to up to 50% of total agricultural output [1], with 11 million tons of crops destroyed every year only in Brazil. Additionally, diseases transmitted by insect vectors are a continuous threat to public health. Malaria, transmitted by the *Anopheles* mosquito, causes more than 300 million acute illnesses and at least one million deaths annually worldwide [2].

Despite ecological concerns, synthetic pesticides remain as the primary tools for implementing insect control. Among the chemical classes that have been developed as pesticides, organophosphorous compounds, together with carbamates, represent the most significant share of the world pesticide market [3]. Both classes owe their acute toxicity to the inhibition of acetylcholinesterase (AChE,[1] acetylcholine hydrolase, EC 3.1.1.7), an enzyme that regulates the concentration of the neurotransmitter acetylcholine (ACh).

Elucidation of the three-dimensional (3D) structure of TcAChE revealed that its active site, located at the bottom of a 20 Å deep gorge, contains a catalytic triad composed of Ser200, His440, and Glu327 residues [4]. Ser200 is suggested to act as a nucleophile towards ACh and His440 is proposed to serve as a general acid–base catalyst, but the catalytic role of Glu327 remains an open question [5]. The X-ray crystallographic structure of the complex between TcAChE and *m*-(*N*,*N*,*N*-trimethylammonio)-2,2,2-trifluoro-acetophenone (TMTFA), a transition state analog inhibitor [6], together with results from kinetic studies with single replacement mutants of AChE (e.g. [7–9]), enabled the identification of a number of subsites that compose the active site, such as the oxyanion hole, the acyl pocket, and the choline binding site, and their relation to the hydrolytic efficiency of the enzyme.

Calculations at various theory levels have been applied to the study of AChE mechanism of action. The influence of specific amino acid residues in the binding of the substrate to AChE and the enzyme specificity were investigated using a combined molecular dynamics and multiple docking approach [10,11]. Both acylation and deacylation steps were evaluated by the semiempirical molecular orbital method with a very simple model of TcAChE [12,13]. Later, the energetics of the acylation step was explored by using an empirical valence bond (EVB) potential surface and an all-atom free energy perturbation (FEP) approach, as well as estimates of the catalytic effect by using the semimicroscope version of the Protein Dipoles Langevin Dipoles method [14]. The deacylation step was also simulated with the complete enzyme using the EVB method in combination with FEP calculations [15]. Molecular dynamics was used to evaluate the active site interactions with tetracoordinate transients in AChE and its mutants [16]. A combined ab initio quantum mechanical/molecular mechanical (QM/MM) approach using a single snapshot from a molecular dynamics trajectory was applied to the study of the acylation step catalyzed by mouse AChE [17], which was followed by a multiple QM/MM reaction path study to investigate the influence of different conformations of the enzyme on the reaction energy barrier [18]. More recently, ab initio quantum mechanics calculations were applied to sim-

[1] *Abbreviations used:* AChE, acetylcholinesterase; DmAChE, *Drosophila melanogaster* acetylcholinesterase; HuAChE, human acetylcholinesterase; TcAChE, *Torpedo californica* acetylcholinesterase; ACh, acetylcholine.

plified active site models to study the acylation step of the AChE-catalyzed reaction [19,20].

The understanding of molecular aspects of insect enzyme mechanisms of action and inhibition can be anticipated as a tool for helping the development of new pesticide leads. Moreover, a comparison between mechanistic aspects of reactions catalyzed by vertebrate and insect AChE may help the development of more selective and secure insecticides in the future. The crystallographic structure of native *Drosophila melanogaster* AChE (DmAChE) revealed some structural differences after comparison with TcAChE, such as in the residues clustered near the opening of the active site gorge, and in the acyl binding pocket, where the residue equivalent to Phe288 in TcAChE is a leucine (Leu328), thus enabling the insect acyl binding pocket to accommodate larger moieties [21].

A suitable molecular description of enzyme-catalyzed reactions requires a theoretical approach capable of evaluation of the breaking and formation of covalent bonds. The use of complete ab initio quantum mechanical calculations to study such systems is limited because a great number of atoms must be considered for evaluation of the effect of the enzymatic environment on the reaction mechanism. This effect was considered at the classical level in studies of the AChE acylation step by the QM/MM method [17,18].

Although the simplifications introduced in semiempirical MO methods limited the accuracy of their results (see [22] and references therein), the computational time scale of these calculations allows the inclusion of many more atoms in the models, which is expected to result in a better description of enzymatic systems than is accessible by high-level quantum methods. In fact, the application of the linear-scaling formalism has expanded the realm of semiempirical calculations to the complete protein level [23]. Improvements have been implemented and are expected to continuously extend the quality and the range of applications of semiempirical methods [24–26].

As part of a program for the development of synthetic substances for pest control, the objective of the present work is the construction of a reliable DmAChE model to provide qualitative information with a low computational cost for helping the future design of pesticide leads. In the present work, we used the semiempirical PM3 molecular orbital method, which was previously employed by us to model an insect enzyme-catalyzed reaction [27], as an alternative approach to the study of AChE-catalyzed reactions. A model composed of first shell active site amino acid residues was used for the evaluation of a complete ACh hydrolysis enzymatic cycle (including the formation of the substrate–enzyme complex, acylation of the enzyme, and deacylation by hydrolysis). The quality of the results obtained here was evaluated by comparison with experimental and theoretical results previously reported in the literature.

2. Computational details

The enzyme model was constructed from entry 1QO9 in the Protein Data Bank [21] by selection of active site residues with the Rasmol 2.6 program [28]. Accordingly, to the results of Fuxreiter and Warshel [14], the most important catalytic effects in AChE are associated with nearby residues rather than distant residues, but some second shell residues were also included in the model (DmAChE-M1), because it is intended for the future design of new pesticide leads. Natural mutations of second shell residues in *D. melanogaster* were shown to confer resistance to insecticides [29]. Water molecules were chosen based on their proximities to the selected amino acid residues. The final model (DmAChE-M1)

was composed by the Cartesian coordinates for Trp83 (Trp84)[2], Gly149 (Gly117), Gly150 (Gly118), Gly151 (Gly119), Ile161 (Val129), Glu237 (Glu199), Ser238 (Ser200), Ala239 (Ala201), Gly265 (Gly227), Trp271 (Trp233), Leu328 (Phe288), Phe330 (Phe290), Glu367 (Glu327), Phe371 (Phe331), His480 (His440), Gly481 (Gly441), and for five water molecules (35, 37, 46, 75, and 104). The truncated peptide bonds were saturated with hydrogen atoms. Hydrogen atoms were added with Sybyl 6.8 program (Tripos Software, Inc.), considering both glutamic acid residues in carboxylate form. The coordinates of the peptide atoms were generally fixed during calculations, with exception of those from residues Ser238 and His480, because motions on these peptide chains were necessary during some steps of the reaction mechanism.

Because H-bonds play a pivotal role in the AChE-catalyzed hydrolysis mechanism, the calculations were done with the PM3 method [31], which is available from the Mopac 6.0 package [32]. PM3 was shown to correctly predict the structure of many types of intermolecular H-bonds [33–36]. This semiempirical method was also shown to predict good geometries for cation–π interactions [37], which were suggested as involved in the interaction between the positively charged group of ACh and Trp86 in TcAChE [8]. To obtain the various stationary points of the hydrolysis pathway, the reaction coordinate method [38] was generally used to render as smooth as possible the geometry change between systems. During the search procedure, convergence and geometry optimization criteria were kept at default values; molecular geometries associated with proposed stationary points of the reaction pathway were further optimized with the Eigenvector Following routine [39] to a gradient norm <0.5 kcal/(Å or rad). All calculations were carried out on Pentium III 1.1 GHz microcomputers.

3. Results and discussion

3.1. Acylation pathway

Scheme 1 presents the steps of the acylation pathway evaluated in this work. The Michaelis complex (system **1**) was obtained after optimization of the structure resulting from the introduction, the substrate with dihedral angles of ca. 180° for both Me_3N^+–C–C–O and C–C–O–COMe inside DmAChE-M1. This conformation resulted in projection of the quaternary ammonium group against the open face of the indole ring of Trp83, in accordance with previous literature results [6].

QM/MM studies with the complete mouse AChE [17,18] and early semiempirical studies with simplified models of bovine trypsin [40] and TcAChE [12,13] active sites indicated a concerted mechanism for the acylation step, involving a simultaneous nucleophilic attack with the proton transfer. On the other hand, results obtained with an interpolated free energy surface for a histidine-catalyzed nucleophilic attack of methanol on formamide indicated a stepwise path, with a shallow surface that could also allow for a concerted path [41]. To investigate with our model the mechanism of Ser238 addition to ACh, we used a simple grid approach with the reaction coordinate method. The effect of His480 as a base was evaluated at six fixed distances of the serine Oγ to the ACh carbonyl carbon (Table 2).

[2] Amino acids and numbers in parentheses refer to the positions of analogous residues in TcAChE according to the recommended nomenclature [30].

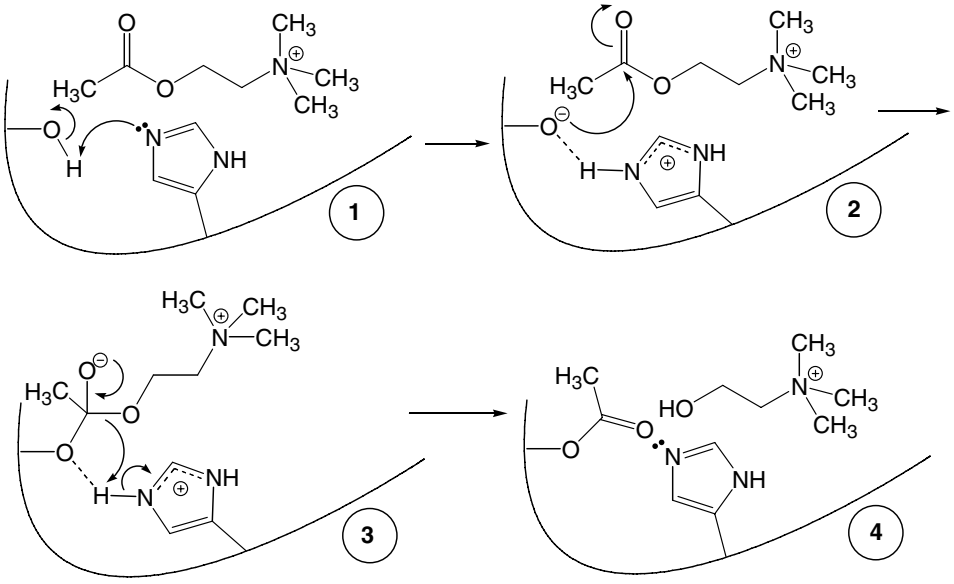

Scheme 1. Steps of the acylation pathway.

The table columns describe the enthalpy profile of the nucleophilic attack of the serine residue with a progressively anionic character towards the substrate. It can be observed that although the attack of the neutral nucleophile (first column) had the lowest initial enthalpy, it increased steadily up to the smallest C–O distance. The lowest enthalpy path (shown in italics in Table 2) involved a partial proton transfer to Nε of His480 at the longer C–O distance, followed by alternated reductions of the C–O and of the N–H distances. Formation of the tetrahedral adduct was complete at the final structure. The stepwise mechanism, represented in our model by the path along the first row of the table followed by a movement down the last column, is disfavored by about 4 kcal/mol compared to the concerted mechanism. In fact, all structures of the minimum enthalpy path are more stable than the last structure of the first row in Table 2, which corresponds to the intermediate of the acylation step in the stepwise mechanism (system**2**). Our model, in accordance with previous results [12,13,40], suggests that the adduct formation is more probable to occur by the concerted mechanism.

It is interesting to observe that the enthalpy barrier is ca. 20 kcal/mol lower than the energetic cost calculated previously by the AM1 method for a similar reaction with an enzymatic model composed solely by TcAChE Ser200 and His440 residues [12]. This result reveals the stabilizing effects of the additional amino acid residues included in our model, which have specific interactions with the substrate (Table 1), such as a H-bond between the peptidic NH group of Gly151 and the carbonyl oxygen of ACh, and cation–π interactions between Trp83 and the substrate ammonium group.

System **3** was obtained directly from system **2** by the reaction coordinate method. Four geometries with different "frozen" internuclear distances (2.5, 2.0, 1.7, and 1.5) between the negatively charged serine Oγ and the ACh carbonyl C atom were calculated, and the final structure was reoptimized with a free C–O distance. In system **3**, the carbonyl C atom became tetrahedral, with a final C–O distance of 1.40 Å (Table 1). As can be seen

Table 1
Relative enthalpies and selected distances of amino acid residues of DMAChE-M1 to the ACh molecule in PM3-calculated systems in the acylation stage

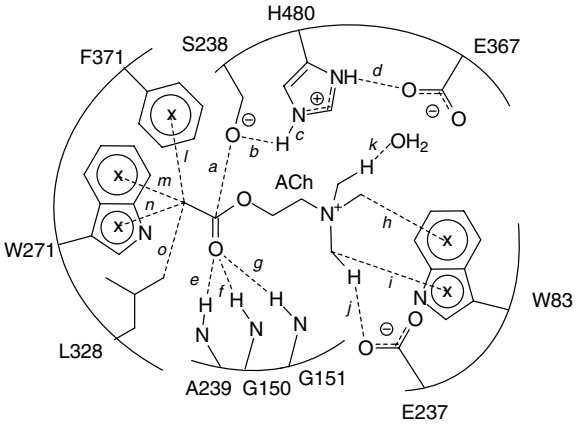

Property[a]	System			
	1	**2**	**3**	**4**
a	2.95	2.54	1.40	1.35
b	0.97	1.59 (166.5)	1.76 (155.4)	—
c	1.79 (164.4)	1.08	1.08	1.76
d	1.71 (165.1)	1.70 (156.5)	1.70 (143.6)	1.72 (176.3)
e	—	—	1.80 (163.6)	1.88 (140.8)
f	—	—	1.81 (159.3)	2.79 (146.6)
g	1.85 (129.0)	1.87 (129.1)	1.64 (170.9)	1.81 (150.0)
h	3.42	3.56	3.86	3.89
i	3.57	3.77	3.74	3.89
j	1.76	2.40	2.88	3.50
k	1.79 (175.6)	1.77 (165.3)	1.79 (172.6)	1.81 (159.4)
l	4.46	4.48	—	—
m	—	4.82	4.20	4.20
n	—	4.57	4.76	3.88
o	3.55	3.56	4.47	4.04
ΔH_f[b]	0.0	35.5	13.0	1.0

[a] Distances in Å; numbers in parenthesis represent H-bond angle.
[b] kcal/mol.

in Table 1, the number of H-bonds formed by the oxyanion hole residues increased as a consequence of the formation of the tetrahedral adduct. The additional H-bonds formed probably help to stabilize the negative charge enhancement on the carbonyl O atom (from −0.44 to −0.74) associated with the carbonyl π bond breaking.

Fig. 1 presents a superposition of system **3** and the corresponding X-ray structure of TMTFA-inhibited TcAChE (code 1AMN in PDB) [6]. The three-pronged oxyanion holes are very similar in both structures. The greatest structural differences are associated to res-

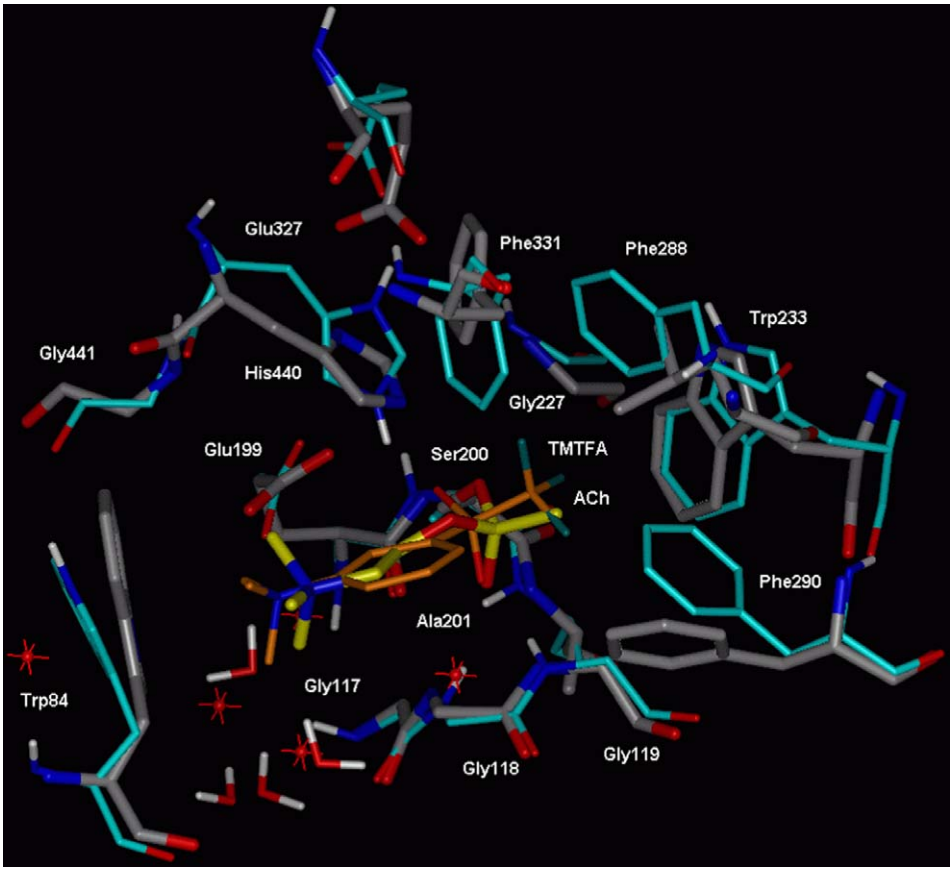

Fig. 1. 3D representation of a superposition of system **3** and the corresponding X-ray structure of TMTFA-inhibited TcAChE [6]. Amino acid numbering refers to TcAChE. Some hydrogen atoms were omitted for clarity. Color code: grey, C (DmAChE); cyan, C (TcAChE); yellow, C (ACh); orange, C (TMTFA); red, O; blue, N; white, H; green, F.

idues of the acyl pocket, which are interacting with groups presenting different volumes and electronic properties, a methyl group in our model and a trifluoromethyl group in the crystallographic structure. Four of the five water molecules included in our model remained in the surroundings of the quaternary ammonium group; the closest distances of approach between their O atoms and methyl C atoms of the cationic group are 2.9, 3.2, 3.4, and 4.1 Å. The crystallographic results showed three water molecules located at 3.2, 3.3, and 3.9 Å from the methyl C atoms of the quaternary ammonium group of TMTFA. In the modeled structure there is a H-bond between Glu367 and His448, with a N–O distance equal to 2.61 Å, which is in excellent agreement with the short H-bond (2.62 ± 0.02 Å) determined by proton NMR data for HuAChE complexed with TMTFA [42].

Manojkumar et al. [20] obtained a second intermediate in the acylation pathway, which contains a H-bond between the protonated histidine and the O atom of the choline moiety. We tried to obtain this second intermediate structure, but all attempts reverted to the system **3**. However, a second intermediate structure where the protonated His480 residue is

H-bonded to the O atom equivalent to that of the choline moiety was easily obtained in the deacylation mechanism (see Section 3.2 below). When we superimpose the structures of the first intermediates of both pathways, a possible reason for this difference could be observed. In order the form the H-bond with the choline O atom, a rotation of His480 side chain is necessary, but this torsion will lead to a collision between the imidazole ring and the choline moiety. This moiety is absent in the deacylation step, so we could obtain the second intermediate structure with no difficulty. Accordingly, we suppose that Manojkumar et al. could obtain the second intermediate in their study of the acylation step because they used a simplified ester to represent the ACh molecule where a small ethoxy group replaces the choline moiety. It is also important to remember that the protonated imidazole ring and the choline ammonium group (which is absent in the model of Manojkumar et al.) are both positively charged, and a strong electrostatic repulsion could be expected as a result of the torsion of the His480 side chain toward the choline moiety. But how does the rupture of the C–O bond occur in the real enzyme? Our results suggest that it is necessary a prior weakening of the bond with no direct participation of the H-bond of the protonated His480 residue. It is possible that the electrostatic repulsion between both positively charged groups helps in this process. Once the C–O bond is weakened, the choline moiety becomes more distant of the His480 side chain, so it could establish a H-bond with the increasingly negative O atom of the choline moiety, which finally collapses as a H–O covalent bond in the leaving group.

The last step of the acylation pathway evaluated was the release of the choline moiety (**3** → **4**), which was accomplished by protonation of the O atom of choline. The reaction coordinate method was employed, with the distance of the His480 H atom bonded to Nε to the choline O atom as the reaction coordinate. Six "frozen" distance (2.4, 2.0, 1.6, 1.4, 1.2, and 1.0 Å) intermediates were calculated, and then the H–O distance was left free in the final geometry during a reoptimization step. As a result of this process, the original ester C–O bond was cleaved, but the choline moiety remained H-bonded to His480 Nε. At this point, all three H-bonds with the carbonyl O atom in the oxyanion hole were weakened (Table 2). Data in Table 2 also suggest that the interactions in the acyl pocket were reinforced in system **4**. The overall calculated enthalpy change between systems **1** and **4** is slightly unfavorable by 1.0 kcal/mol.

It is interesting to observe that Glu237 apparently did not play any important role during the acylation pathway: its distance to one of the methyl substituents of the quaternary ammonium group increased during the sequence **1** → **3** → **4** (Table 1). This result may be related to experimental results on TcAChE which showed that the mutation of the corre-

Table 2
PM3 calculated relative ΔH_f (kcal/mol) along the reaction pathway for formation of the first tetrahedral intermediate

ACh C–Oγ Ser203 distance (Å)	His480 Nε–HO Ser203 distance (Å)					
	1.60	1.50	1.40	1.30	1.20	1.10
2.95	*0.0*	*4.1*	*8.6*	15.2	22.0	28.4
2.50	13.4	16.4	14.8	20.4	26.0	32.4
2.10	10.0	12.5	*18.3*	*21.6*	27.4	28.3
1.80	16.5	18.6	22.7	*26.7*	29.9	24.4
1.60	22.3	23.3	26.0	*28.2*	*22.8*	*17.3*
1.45	28.0	29.8	30.8	32.7	19.3	*14.5*

Numbers in italics represent the lowest enthalpy path.

sponding Glu199 residue to Gln leads to only a fourfold decrease in k_{cat} [43]. However, because of the H-bond formed between the carboxylate group of Glu237 and one of the methyl groups of the ACh ammonium group in system **1** (see Table 1), it can be concluded that Glu237 effectively contributes to the substrate binding, which is in accordance to the results obtained by Kua et al. [10]. The corresponding N–O distance is 3.99 Å, which is in fair agreement with the average distance (3.82 Å) obtained by Kua et al.

3.2. Deacylation pathway

For the second reaction stage, the calculated steps are shown in (Scheme 2). Departure of choline from the active site should involve dynamic events not amenable with the present model, so the starting structure for the deacylation modeling was generated by removal of the choline moiety from the model (Table 3). This approach is justifiable by experimental results, which indicate that the release of thiocholine is faster than the deacylation in the inhibition of AChE by thiocholine [44].

Following a geometry optimization of this new system, **5**, the deacylation mechanism was started by manually changing the position of the water molecule nearest to the substrate C atom bonded to Ser238 Oγ atom. One of the hydrogen atoms of this water molecule was pointed toward the lone pair of His480 Nε. As before, this residue is expected to act as an internal base to abstract a proton from the nucleophilic reagent, which is now the water molecule. The geometry was then reoptimized and the resulting system (**6**) was ca. 6 kcal/mol more stable than the previous one.

Based on the results obtained in the acylation pathway, we explored the concertedness of the mechanism for the formation of the second tetrahedral intermediate. The grid approach was used to evaluate the proton transfer from the water molecule to the His480 Nε at fixed distances of the carbonyl C atom to the water O atom (Table 4). Unlike the previous mechanism, the lowest enthalpy path involved the approximation between the nucleophile and the substrate without a great transfer of the proton to the imidazole ring. This transfer occurred after the carbonyl carbon and the water oxygen are very close

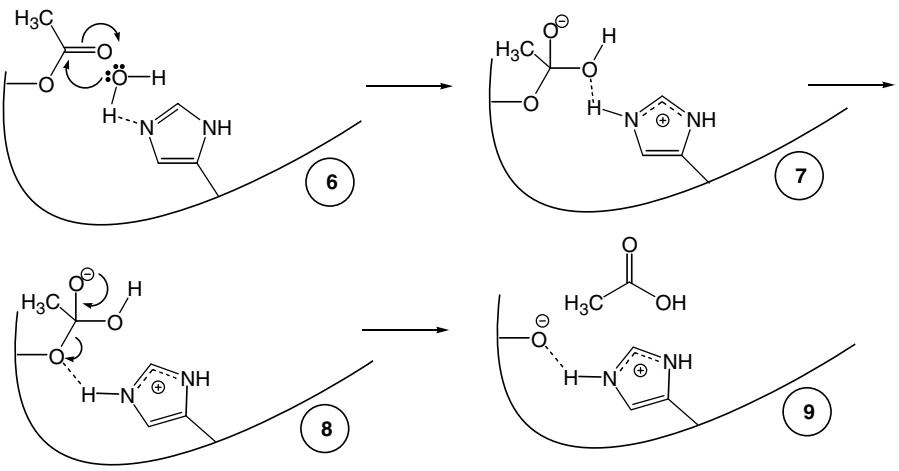

Scheme 2. Steps of the deacylation pathway.

Table 3
Relative enthalpies and selected distances of interacting groups in amino acid residues of DMAChE-M1 to the substrate molecule in PM3-calculated systems in the deacylation stage

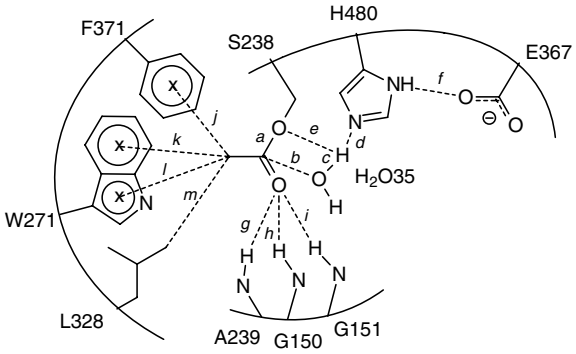

Property[a]	System			
	6	**7**	**8**	**9**
a	1.35	1.43	1.43	3.25
b	3.37	1.43	1.43	1.34
c	0.98	1.80 (139.6)	2.49	2.89
d	1.78 (168.8)	1.01	1.01	1.78 (165.1)
e	—	2.66	1.79 (133.6)	0.97
f	1.74 (173.3)	1.70 (166.9)	1.69 (168.1)	1.72 (166.6)
g	1.81 (153.5)	1.75 (160.8)	1.74 (161.8)	—
h	2.84 (142.6)	2.65 (151.0)	2.73 (149.8)	—
i	1.88 (141.6)	1.70 (155.3)	1.70 (148.6)	—
j	—	—	—	4.80
k	4.32	4.71	3.63	3.76
l	4.58	4.80	4.45	4.31
m	3.94	3.97	4.65	3.75
ΔH_f[b]	0.0	4.3	5.9	−10.1

[a] Distances in Å; numbers in parenthesis represent H-bond angle.
[b] kcal/mol.

Table 4
Calculated relative ΔH_f (kcal/mol) along the reaction pathway for formation of the second tetrahedral intermediate

ACh C–OH2 distance (Å)	His480 Nε–HOH distance (Å)					
	1.60	1.50	1.30	1.20	1.10	1.00
3.37	*0.0*	4.6	17.8	33.2	36.5	36.5
2.90	*0.9*	5.4	18.0	24.9	32.6	32.9
2.40	*5.2*	9.5	21.2	32.0	34.4	34.4
2.20	*8.8*	*2.4*	22.3	27.8	30.8	30.1
1.80	15.4	*17.6*	24.7	20.2	18.4	19.7
1.60	18.9	*20.8*	25.2	11.4	8.9	8.9
1.45	23.8	*24.5*	*21.5*	*6.7*	*4.0*	*4.0*

Numbers in italics represent the lowest enthalpy path.

together to produce the second tetrahedral adduct with a protonated histidine residue. Finally, both distances were left free and the geometry was reoptimized, yielding the second tetrahedral intermediate (**7**). Once again, H-bonds formed with the amino acids of the oxyanion hole helped the formation of the tetrahedral adduct (Table 3), but now the complete **6** → **7** transformation was unfavorable by 4.3 kcal/mol. It can be observed that a process involving a proton transfer to the histidine residue before the nucleophilic attack (last column in Table 4) would be clearly disfavored, since the initial structure has a high heat of formation.

To change the acceptor of the His480-H^+H-bond from the OH group to the Ser238 Oγ atom, the dihedral angles of His480-H^+ side chain were replaced in system **7** by those observed in system **4**. After optimization, this new conformation resulted in a slightly less stable system (**8**), in which His480-H^+ became H-bonded to the serine Oγ atom (Table 3). The same kind of asymmetric H-bonds observed in systems **7** and **8** were also obtained in a study of the deacylation step of another serine protease (porcine pancreatic elastase) using QM/MM dynamics in conjunction with umbrella sampling [45]. In this work, the calculated histidine NεH···OH and the histidine NεH···OR average distances are, respectively, 1.63 ± 0.12 and 2.20 ± 0.03 Å in the first intermediate, which corresponds to system **7** (where the respective distances are 1.80 and 2.66 Å), and 2.43 ± 0.20 and 1.64 ± 0.11 Å in the second intermediate, which corresponds to system **8** (where the distances are 2.49 and 1.79 Å, respectively).

The final geometry of the deacylation stage was obtained by simulation of the acetic acid departure from the tetrahedral adduct at six fixed C–O distances (1.4, 1.5, 1.7, 2.0, 2.2, and 2.5 Å). System **9** was obtained by a reoptimization of the last geometry with a free C–O distance. This system, in which the acetic acid molecule is completely detached from the serine Oγ atom, is 16 kcal/mol more stable than the previous one. Based on the results obtained in the **1** → **2** transformation, the greatest contribution on this result should be the fact that now both Ser238 and His480 are in neutral form. However, amino acids of the acyl pocket should also contribute to this process, as can be seen by the movement of the methyl group of the product towards apolar side chains (Table 3). The overall calculated enthalpy change between systems **5** and **9** was −16.22 kcal/mol.

4. Conclusions

The present simplified model suitably describes the expected behavior for the ACh hydrolysis catalyzed by the AChE enzyme. The structural and energetic profiles for the hydrolysis of ACh in *D. melanogaster* AChE calculated by the semiempirical approach were generally in accordance with experimental and theoretical results obtained previously with vertebrate AChEs. The major difference was observed in the structure of the Michaelis complex. Zhang et al. have observed with the QM/MM approach that both H-bonds formed by the oxyanion hole glycine residues were already present in the mouse AChE Michaelis complex [15]. The reason for this difference possibly resides on the change of an amino acid residue between insect and vertebrate AChEs, Leu328, which is a phenylalanine in the latter. This residue replacement renders the DmAChE acyl pocket less rigid [17]; the capability of insect AChEs to hydrolyze substrates with larger acyl moieties, such as butyrylcholine, is known [46]. Because the esteratic methyl group of ACh can be accommodated deeper in the acyl pocket, the substrate carbonyl group is positioned farther from the oxyanion hole in the insect enzyme in comparison with the mouse enzyme.

Formation of the first tetrahedral intermediate is the result of a nucleophilic addition of Ser238 to the carbonyl group of the substrate. The catalytic role of His480 is apparently to reduce the energetic cost for this nucleophilic attack by a simultaneous proton transfer from Ser238 to the Nε of the histidine residue. The third residue of the catalytic triad, Glu237, interacts with the imidazole group of His480 by means of a H-bond. All three residues of the oxyanion hole were found to stabilize the covalent complex by means of H-bonds. A proton transfer from the protonated histidine to the choline O atom resulted in the breakdown of the bond between this atom and the substrate carbonyl C atom. After the bond rupture, the acyl group moves towards the side chains of amino acids of the acyl pocket, suggesting a favorable participation of these groups by dispersion forces.

In the deacylation pathway, formation of the tetrahedral intermediate is also helped by three H-bonds within the oxyanion hole, but differently from the corresponding step in the acylation mechanism, this initial step is predicted as slightly unfavorable by our model. The reaction profile obtained for the formation of the tetrahedral intermediates from both pathways revealed that when the nucleophile is Ser238, a more complete proton transfer to His440 occurs before the nucleophilic attack, as compared to the water nucleophile. A possible explanation for this difference is a stabilization of the increasing negative charge of the serine residue caused by the field effect of the adjacent positive charge of the ammonium group of ACh. Formation of the product is an exothermic step, rendering the complete sequence for the enzyme deacylation, a favorable process. Amino acid residues Trp271 and Leu328 of the acyl pocket probably contribute to stabilize the departure of acetic acid from the serine residue, but the main driving force should be the return of His480 and Ser238 to their neutral forms.

Acknowledgments

The Brazilian National Council of Research (CNPq) and the FAPERJ Foundation are acknowledged for financial support. LASSBio/UFRJ is acknowledged for the use of computational facilities.

References

[1] A. Shani, Chemtech 28 (1998) 30–35.
[2] http://www.who.int/inf-fs/en/InformationSheet01.pdf, 2003.
[3] J.E. Casida, G.B. Quistad, Annu. Rev. Entomol. 43 (1998) 1–16.
[4] J.L. Sussman, M. Harel, F. Frolow, C. Oefner, A. Goldman, L. Toker, I. Silman, Science 253 (1991) 872–879.
[5] D. Quinn, R. Medhekar, N. Baker, Ester Hydrolysis. In Comprehensive Natural Products Chemistry: Enzymes, Enzyme Mechanisms, Proteins, and Aspects of NO Chemistry, Elsevier Science, Oxford, 1999.
[6] M. Harel, D.M. Quinn, H.K. Nair, I. Silman, J.L. Sussman, J. Am. Chem. Soc. 118 (1996) 2340–2346.
[7] A. Shafferman, B. Velan, A. Ordentlich, C. Kronman, H. Grosfeld, M. Leitner, Y. Flashner, S. Cohen, D. Barak, N. Ariel, EMBO J. 11 (1992) 3561–3568.
[8] A. Ordentlich, D. Barak, C. Kronman, Y. Flashner, M. Leitner, Y. Segall, N. Ariel, S. Cohen, B. Velan, A. Shafferman, J. Biol. Chem. 268 (1993) 17083–17095.
[9] A. Ordentlich, D. Barak, C. Kronman, N. Ariel, Y. Segall, B. Velan, A. Shafferman, J. Biol. Chem. 273 (1998) 19509–19517.
[10] J. Kua, Y. Zhang, J.A. McCammon, J. Am. Chem. Soc. 124 (2002) 8260–8267.
[11] J. Kua, Y. Zhang, A. Eslami, J.R. Butler, J.A. McCammon, Protein Sci. 12 (2003) 2675–2684.
[12] Q.M. Wang, H.L. Jiang, J.Z. Chen, K.X. Chen, R.Y. Ji, Int. J. Quantum Chem. 70 (1998) 515–525.
[13] Q.M. Wang, H.L. Jiang, K.X. Chen, R.Y. Ji, Y.J. Ye, Int. J. Quantum Chem. 74 (1999) 315–325.

[14] M. Fuxreiter, A. Warshel, J. Am. Chem. Soc. 120 (1998) 183–194.
[15] P. Vagedes, B. Rabenstein, J. Åqvist, J. Marelius, E.-W. Knapp, J. Am. Chem. Soc. 122 (2000) 12254–12262.
[16] I.J. Enyedy, I.M. Kovach, A. Bencsura, Biochem. J. 353 (2001) 645–653.
[17] Y. Zhang, J. Kua, J.A. McCammon, J. Am. Chem. Soc. 124 (2002) 8260–8267.
[18] Y. Zhang, J. Kua, J.A. McCammon, J. Phys. Chem. B 107 (2003) 4459–4463.
[19] H. Tachikawa, M. Igarashi, J. Nishihira, T. Ishibashi, J. Photochem. Photobiol. B 79 (2005) 11–23.
[20] T.K. Manojkumar, C. Cui, K.S. Kim, J. Comput. Chem. 26 (2005) 606–611.
[21] M. Harel, G. Kryger, T.L. Rosenberry, W.D. Mallender, T. Lewis, R.J. Fletcher, J.M. Guss, I. Silman, J.L. Sussman, Protein Sci. 9 (2000) 1063–1072.
[22] W. Harb, M.I. Bernal-Uruchurtu, M.F. Ruiz-López, Theor. Chem. Acc. 112 (2004) 204–216.
[23] J.J.P. Stewart, J. Mol. Struct. (THEOCHEM) 401 (1997) 195–205.
[24] T. Clark, J. Mol. Struct. (THEOCHEM) 530 (2000) 1–10.
[25] J.J.P. Stewart, J. Mol. Mod. 10 (2004) 155–164.
[26] T. Bredow, K. Jug, Theor. Chem. Acc. 113 (2005) 1–14.
[27] C.M.R. Sant'Anna, V.P. Souza, D.S. Andrade, Int. J. Quantum Chem. 87 (2002) 311–321.
[28] R. Sayle, Glaxo Wellcome Research and Development, Stevenage, Hertfordshire, UK, 1993.
[29] A. Mutero, M. Pralavorio, J.-M. Bride, D. Fournier, Proc. Natl. Acad. Sci. USA 91 (1994) 5922–5926.
[30] J. Massouline, J.L. Sussman, B.P. Doctor, H. Soreq, B. Velan, M. Cygler, R. Rotundo, A. Shafferman, I. Silman, P. Taylor, in: A. Shafferman, B. Velan (Eds.), Multidisciplinary Approaches to Cholinesterase Functions, Plenum Publishing Corp, New York, 1992, pp. 285–288.
[31] J.J.P. Stewart, J. Comp. Chem. 10 (1989) 209–220.
[32] J.J.P. Stewart, QCPE 455, available from Indiana University Bloomington, USA, 1992.
[33] S. Schröder, V. Daggett, P. Kollman, J. Am. Chem. Soc. 113 (1991) 8922–8925.
[34] Y.-J. Zheng, K.M. Merz Jr., J. Comp. Chem. 13 (1992) 1151–1169.
[35] M.W. Jurema, G.C. Shields, J. Comp. Chem. 14 (1993) 89–104.
[36] T.N. Lively, M.W. Jurema, G.C. Shields, Int. J. Quant. Chem., Quant. Biol. Symp. 21 (1994) 95–107.
[37] C.M.R. Sant'Anna, E.J. Barreiro, R.B. Alencastro, J. Mol. Struct. (THEOCHEM) 429 (1998) 217–227.
[38] M.J.S. Dewar, S. Kirschner, J. Am. Chem. Soc. 93 (1971) 4290.
[39] J. Baker, J. Comput. Chem. 7 (1986) 385–395.
[40] V. Daggett, S. Schröder, P. Kollman, J. Am. Chem. Soc. 113 (1991) 8926–8935.
[41] M. Strajbl, J. Florián, A. Warshel, J. Am. Chem. Soc. 122 (2000) 5354–5366.
[42] M.A. Massiah, C. Viragh, P.M. Reddy, I.M. Kovach, J. Johnson, T.L. Rosenberry, A.S. Mildvan, Biochemistry 40 (2001) 5682–5690.
[43] Z. Radic, G. Gibney, S. Kawamoto, K. MacPhee-Quigley, C. Bongiorno, P. Taylor, Biochemistry 31 (1992) 9760–9767.
[44] T. Szegletes, W.D. Mallender, P.J. Thomas, T.L. Rosenberry, Biochemistry 38 (1999) 122–133.
[45] M. Topf, W.G. Richards, J. Am. Chem. Soc. 126 (2004) 14631–14641.
[46] A.L. Gnagey, M. Forte, T.L. Rosenberry, J. Biol. Chem. 262 (1987) 13290–13298.